Inorganic Chemistry

Article

pubs.acs.org/IC

Oxonitridosilicate $Y_{10}(Si_6O_{22}N_2)O_2:Ce^{3+},Mn^{2+}$ Phosphors: A Facile Synthesis via the Soft-Chemical Ammonolysis Process, Luminescence, and Energy-Transfer Properties

Dongling Geng,[†,‡] Hongzhou Lian,[†] Mengmeng Shang,[†] Yang Zhang,[†,‡] and Jun Lin*[,†]

[†]State Key Laboratory of Rare Earth Resource Utilization, Changchun Institute of Applied Chemistry, Chinese Academy of Sciences, Changchun 130022, People's Republic of China

[‡]University of Chinese Academy of Sciences, Beijing 100049, People's Republic of China

Supporting Information

ABSTRACT: Ce^{3+}- and/or Mn^{2+}-activated $Y_{10}(Si_6O_{22}N_2)O_2$ phosphors have been prepared via a soft-chemical ammonolysis method. Structure refinement, scanning electron microscopy, high-resolution transmission electron microscopy, energy-dispersive X-ray spectroscopy, Fourier transform infrared, and thermogravimetry analysis have been employed to characterize the phase purity, crystal structure, morphology, crystallization condition, chemical composition, and thermal stability of the products. The photoluminescence and cathodoluminescence properties for Ce^{3+}- and Mn^{2+}-doped $Y_{10}(Si_6O_{22}N_2)O_2$ phosphors were studied in detail. For Ce^{3+}/Mn^{2+} singly doped $Y_{10}(Si_6O_{22}N_2)O_2$ phosphors, typical emissions of Ce^{3+} (blue) and Mn^{2+} (reddish-orange) ions can be observed. Especially, Ce^{3+} emission at different lattice sites 4f and 6h has been identified and discussed. Energy transfer from Ce^{3+}(I) and Ce^{3+}(II) to Mn^{2+} ions in $Y_{10}(Si_6O_{22}N_2)O_2:Ce^{3+},Mn^{2+}$ samples has been validated and confirmed by the photoluminescence spectra and luminescence decay times. A color-tunable emission in $Y_{10}(Si_6O_{22}N_2)O_2:Ce^{3+},Mn^{2+}$ phosphors can be achieved by an energy-transfer process and a change in the doping concentration of the activators. The temperature-dependent photoluminescence properties and degradation property of cathodoluminescence under continuous electron bombardment of as-synthesized phosphors prove that the $Y_{10}(Si_6O_{22}N_2)O_2$ host has good stability. Therefore, the $Y_{10}(Si_6O_{22}N_2)O_2:Ce^{3+},Mn^{2+}$ phosphors may potentially serve as single-phase blue/reddish-orange phosphors for white-light-emitting diodes and field-emission displays.

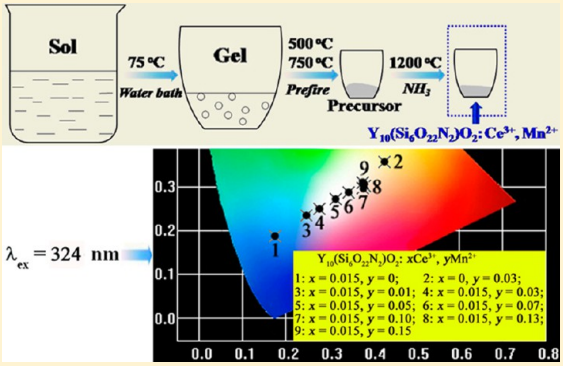

1. INTRODUCTION

In the current background of global energy shortages, energy conservation is the important issue we have to face. Recently, white-light-emitting diodes (W-LEDs) have drawn lots of attention because they have many advantages compared with incandescent and fluorescent lamps, such as energy savings, long lifetime, small volume, and free from toxicity.[1] The lack of a red component for the classical W-LEDs combined with a blue InGaN LED chip and the yellow phosphor YAG:Ce^{3+} brought out many problems including a poor color-rendering index and high correlated color temperature.[2] Therefore, it is a pressing task to explore and develop red-emitting luminescent materials that exhibit high stability in both brightness and chromaticity. Besides, the phosphors that can give excellent white-light emission directly in a single host could solve the problems mentioned in W-LEDs.[3] At the same time, field-emission displays (FEDs) attract considerable attention because of several charming features, such as thin-panel thickness, self-emissivity, quick responses, distortion of the free image, and a wide viewing angle (170°).[4] Because power is theoretically consumed only at the emitting part, FEDs are also accounted for as low-power-consuming devices.[5] However, the available phosphors for FEDs cannot perfectly adapt the harsh operation conditions.[6] So, advanced phosphors with high quality need to be developed to meet the demands of LEDs and FEDs.

Because of their excellent chemical stability, compounds with an apatite structure (space group $P6_3/m$) have been regarded as effective host lattices for luminescent materials because of their applications in the medical field, solid-state lighting industry, and display areas.[7] The two different crystallographic sites, i.e., the nine-coordinated 4f site with C_3 point symmetry and the seven-coordinated 6h site with C_s point symmetry, are the most prominent structural characteristics of the apatite host lattice.[8] Both sites are very suitable for luminescence of rare-earth ions (f–f transitions). A large amount of research has focused on rare-earth ions and Mn^{2+}-activated silicate with the apatite structure, which proves that the apatite structure doped with suitable activators can served as a potential phosphor applied in

Received: November 24, 2013
Published: January 28, 2014

   dx.doi.org/10.1021/ic402916b | *Inorg. Chem.* 2014, 53, 2230–2239

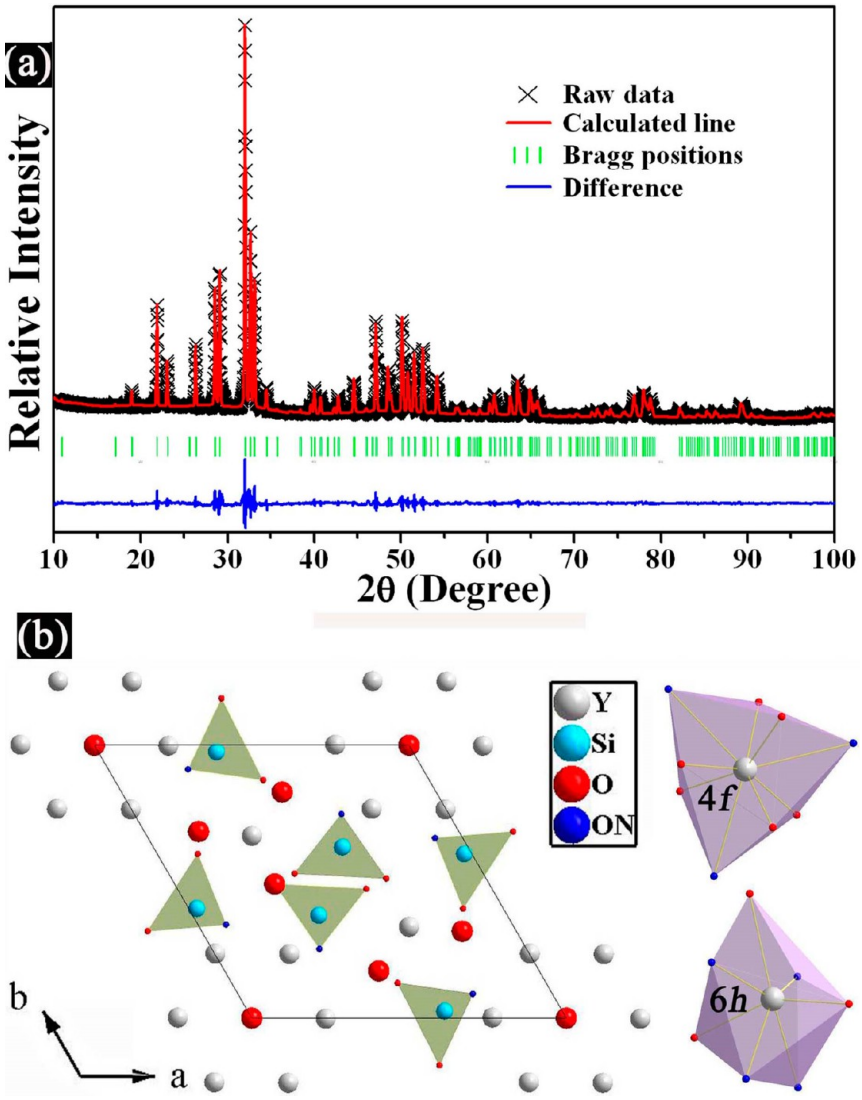

Figure 1. Rietveld refinement of the powder XRD pattern (a) and the crystal structure (b) of $Y_{10}(Si_6O_{22}N_2)O_2$.

W-LEDs.[9] On the other hand, the structure of nitridosilicate typically consists of SiN_4 tetrahedra, which can be partially replaced by $Si[O/N]_4$ tetrahedra. The SiN_4 or $Si[O/N]_4$ units are stacked together by sharing their corners or edges to form a condensed framework, resulting in the chemical stability and excellent thermal stability of nitridosilicate and oxonitridosilicate.[10] Compared with silicate phosphors, oxonitridosilicate phosphors usually have longer-wavelength excitation (emission) bands and excellent stability toward oxidation, hydrolysis, and high temperature.[11] The strong crystal fields and high covalency of the crystal lattices of oxonitridosilicate are responsible for this observation.[12] In the Y−Si−O−N quaternary system, $Y_{10}(Si_6O_{22}N_2)O_2$ belongs to the family of apatite compounds. So, excellent luminescence is expected in rare-earth ions and Mn^{2+}-doped $Y_{10}(Si_6O_{22}N_2)O_2$ phosphors. However, the synthesis of oxonitridosilicates always needs critical synthesis conditions, such as high temperature and high pressure.[13] Also, costly Si_3N_4 is usually chosen as the resource of nitrogen in the compound.[14] Hence, exploring a more convenient, moderate, and less expensive method to synthesize oxonitridosilicates is necessary in further research.

In this report, the $Y_{10}(Si_6O_{22}N_2)O_2$ and $Y_{10}(Si_6O_{22}N_2)$-O_2:Ce^{3+},Mn^{2+} samples with apatite structure have been prepared by a facile, low-cost, and time-saving method. First, we synthesized the precursors for the desired products using the Pechini-type sol−gel process at low temperature. Then, ammonolysis of the precursors was conducted to obtain the final phosphors. Compared with the traditional solid-state high-temperature method, the technique used in our study can be operated in much more mild conditions with low energy consumption. Thomas et al. have prepared $La_{10-x}Sr_x(Si/Ge)_6O_{27-x/2-3y/2}N_y$ phosphors by the ammonolysis of the oxysilicate or oxygermanate precursors which were obtained by high temperature solid state reaction.[15] However, the sintering time is too long (156 h in total), and the sintering temperature is very high (1350−1450 °C) in the preparation of the precursors. In our method, the precursors were synthesized by prefiring the gels at 500 °C for 2 h and then calcining at 750 °C for 4 h in air. So, our method has the advantage of lowering both the sintering time and temperature. The phase purity, crystal structure, particle size, crystallization, and chemical composition of as-synthesized powders have been characterized by General Structure Analysis System (GSAS) refinement, scanning electron microscopy, high-resolution transmission electron microscopy, Fourier transform infrared, and energy-dispersive X-ray techniques. The thermogravimetry analysis

dx.doi.org/10.1021/ic402916b | Inorg. Chem. 2014, 53, 2230−2239

curves, temperature-dependent photoluminescence, and degradation of cathodoluminescence were investigated to determine the stability of the products. The photoluminescence properties for Ce^{3+}(I) and Ce^{3+}(II) located at the 4f and 6h sites and the energy-transfer properties from Ce^{3+}(I) and Ce^{3+}(II) to Mn^{2+} in the $Y_{10}(Si_6O_{22}N_2)O_2$ host under ultraviolet (UV) light and low-voltage electron-beam excitation have been discussed carefully.

2. EXPERIMENTAL SECTION

2.1. Materials. Y_2O_3 (99.999%) was purchased from Science and Technology Parent Company of Changchun Institute of Applied Chemistry, and other chemicals were purchased from Beijing Chemical Company. All chemicals were of analytical grade and were used directly without further purification.

2.2. Preparation. Polycrystalline samples of $Y_{10}(Si_6O_{22}N_2)O_2$ and Ce^{3+}- and/or Mn^{2+}-doped $Y_{10}(Si_6O_{22}N_2)O_2$ were prepared by the Pechini-type sol–gel method followed by ammonolysis of the precursors. First, Y_2O_3 was dissolved in dilute nitric acid (HNO_3) under stirring and heating, resulting in the formation of a colorless solution of $Y(NO_3)_3$. Stoichiometric amounts of $Y(NO_3)_3$, $Ce(NO_3)_3 \cdot 6H_2O$, and $Mn(CH_3COO)_2$ were dissolved in deionized water, with stirring for 15 min, followed by the addition of citric acid in the above solution [2:1 (mol/mol) citric acid/metal ion]. Then, the pH of the solution was adjusted to ~1 with HNO_3 followed by the addition of a stoichiometric amount of tetraethyl orthosilicate, which was dissolved in ethanol. Finally, a certain amount of poly(ethylene glycol) (PEG; molecular weight = 20000, analytical reagant grade) was added as a cross-linking agent (C_{PEG} = 0.01 mol/L) after stirring for several minutes. The resultant mixtures were stirred for 2 h and then heated at 75 °C in a water bath until homogeneous gels formed. The gels were prefired at 500 °C for 2 h in air. Then the samples were fully ground and calcined at 750 °C in air for 4 h. The obtained precursors were treated at a temperature of 1200 °C for 5 h under a NH_3 atmosphere to produce the final oxonitridosilicates.

2.3. Characterization. The X-ray diffraction (XRD) measurements were carried out on a D8 Focus diffractometer using Cu Kα radiation (λ = 0.15405 nm). Structure refinement was done using the GSAS program.[16] Scanning electron microscopy (SEM) micrographs and energy-dispersive X-ray (EDX) spectra were obtained using a field-emission scanning electron microscope (Philips XL30). High-resolution transmission electron microscopy (HRTEM) was performed using a PEI Tecnai G2 S-Twin microscope with a field-emission gun operating at 200 kV. Images were acquired digitally on a Gatan multiople CCD camera. Fourier transform infrared (FTIR) spectra were measured on a Vertex Perkin-Elmer 580BIR spectrophotometer (Bruker) with the KBr pellet technique. Thermogravimetry analysis (TGA) was carried out on a Netzsch STA 409 thermoanalyzer with a heating rate of 10 °C/min in air and nitrogen atmospheres. Photoluminescence (PL) measurements were performed on a Hitachi F-7000 spectrophotometer equipped with a 150 W xenon lamp as the excitation source. The temperature-dependent (300–500 K) PL spectra were obtained on a fluorescence spectrophotometer equipped with a 450 W xenon lamp as the excitation source (Edinburgh Instruments FLSP-920) with a temperature controller. Cathodoluminescence (CL) measurements were carried out in an ultrahigh-vacuum chamber (<10^{-8} Torr), where the phosphors were excited by an electron beam, and the emission spectra were recorded using an F-7000 spectrophotometer. The luminescence decay curves were obtained from a Lecroy Wave Runner 6100 digital osilloscope (1 GHz) using a tunable laser (pulse width = 4 ns; gate = 50 ns) as the excitation (Contimuum Sunlite OPO).

3. RESULTS AND DISCUSSION

3.1. Crystallization Conditions and Morphology. The XRD pattern of the $Y_{10}(Si_6O_{22}N_2)O_2$ sample was defined by GSAS refinement. The starting model was built with crystallographic data taken from ISCD-91850 for the structure of $La_{10}(Si_6O_{22}N_2)O_2$. The experimental, calculated, and difference XRD profiles and Bragg positions for the Rietveld refinement of $Y_{10}(Si_6O_{22}N_2)O_2$ at room temperature are shown in Figure 1a. The pure $Y_{10}(Si_6O_{22}N_2)O_2$ crystallizes hexagonally with space group $P6_3/m$ with $a = b = 9.381$ Å, $c = 6.7723$ Å, $V = 516.14$ Å^3, $\alpha = \beta = 90°$ and $\gamma = 120°$. All atom positions, fraction factors, and thermal vibration parameters were refined by convergence and satisfied well the reflection conditions, R_p = 5.13%, R_{wp} = 6.26%, and χ^2 = 3.79 (Table S1 in the Supporting Information, SI). Figure 1b displays the crystal structure of $Y_{10}(Si_6O_{22}N_2)O_2$ and the coordination environments of the Y^{3+}(I) (4f site) and Y^{3+}(II) (6h site) ions. Obviously, two different crystallographic sites in the $Y_{10}(Si_6O_{22}N_2)O_2$ structure can be distinguished: 4f (C_3) and 6h (C_s). The 4f site with nine-coordination needs large cations for its capacious space, while the 6h site with seven-coordination is favorable for high charge cations.[17] Ce^{3+} has a larger ionic radius [1.07 Å for coordination number (CN) = 7 and 1.196 Å for CN = 9][18] and higher charge (3+), which is suitable for both the 4f and 6h sites. So, the doped Ce^{3+} ions can occupy the two sites simultaneously in the $Y_{10}(Si_6O_{22}N_2)O_2$ structure. According to previous discussions from the points of the electrostatic bond strength and Pauling's electrostatic valence principle,[19] we can infer that the 6h site has little possibility to adopt the cations with low charge. Hence, the Mn^{2+} ions have to occupy the 4f sites (CN = 9) in the $Y_{10}(Si_6O_{22}N_2)O_2$ host.

Figure 2a compares the XRD patterns for $Y_{10}(Si_6O_{22}N_2)O_2$:0.015Ce^{3+}, $Y_{10}(Si_6O_{22}N_2)O_2$:0.05Mn^{2+}, and $Y_{10}(Si_6O_{22}N_2)O_2$:0.015Ce^{3+},0.07Mn^{2+} samples to the calculated pattern for $Y_{10}(Si_6O_{22}N_2)O_2$ obtained by GSAS refinement. From the patterns, we can determine that the desired single-phase phosphors with hexagonal structure have been synthesized and

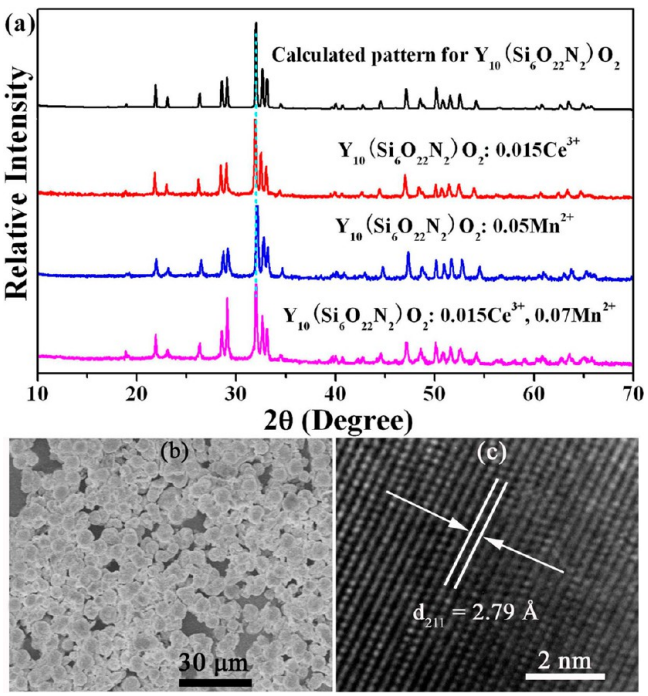

Figure 2. (a) Calculated pattern for the $Y_{10}(Si_6O_{22}N_2)O_2$ host and XRD patterns for the $Y_{10}(Si_6O_{22}N_2)O_2$:0.015Ce^{3+}, $Y_{10}(Si_6O_{22}N_2)O_2$:0.05Mn^{2+}, and $Y_{10}(Si_6O_{22}N_2)O_2$:0.015Ce^{3+},0.07Mn^{2+} samples and (b) SEM and (c) HRTEM images of the as-prepared $Y_{10}(Si_6O_{22}N_2)O_2$ sample, respectively.

dx.doi.org/10.1021/ic402916b | Inorg. Chem. 2014, 53, 2230–2239

the patterns could not be changed by altering the doping activators (Ce^{3+} and Mn^{2+} ions). No impurity peaks were detected. However, the diffraction peak positions of the $Y_{10}(Si_6O_{22}N_2)O_2$:0.05Mn^{2+} sample shift to a high diffraction degree in contrast with that for the calculated pattern for $Y_{10}(Si_6O_{22}N_2)O_2$. This observation can be attributed to the smaller ionic radius of Mn^{2+} with respect to Y^{3+},[18] implying that the obtained samples are single phase and adopt the same structure as the $Y_{10}(Si_6O_{22}N_2)O_2$ host. However, no peak shift was observed in the $Y_{10}(Si_6O_{22}N_2)O_2$:0.015Ce,0.07Mn sample. In the $Y_{10}(Si_6O_{22}N_2)O_2$ host, both Ce^{3+} and Mn^{2+} ions substitute the Y^{3+} site. The relationship of the ionic radii for Ce^{3+}, Y^{3+}, and Mn^{2+} ions is $R_{Ce^{3+}} > R_{Y^{3+}} > R_{Mn^{2+}}$.[18] The doped Ce^{3+} ions can enlarge and the Mn^{2+} ions will reduce the cell parameters of the crystal structure for $Y_{10}(Si_6O_{22}N_2)O_2$. With these two opposite effects, no shift was observed in the $Y_{10}(Si_6O_{22}N_2)O_2$:0.015Ce,0.07Mn sample, which is a predictable result. Figure 2b shows the SEM picture of the as-prepared $Y_{10}(Si_6O_{22}N_2)O_2$. The powder consists of nearly spherical and well-dispersed particles with size ranging from 3 to 8 μm diameter. The clear lattice fringes in the HRTEM image displayed in Figure 2c indicate the high crystallinity of the as-prepared sample. The distance between the adjacent fringes was estimated to be 2.79 Å, corresponding well with the d_{211} spacing (2.8 Å) of the pure $Y_{10}(Si_6O_{22}N_2)O_2$ phase.

Figure 3a depicts the FTIR spectra of the precursor for the $Y_{10}(Si_6O_{22}N_2)O_2$ and $Y_{10}(Si_6O_{22}N_2)O_2$ samples. The precursor

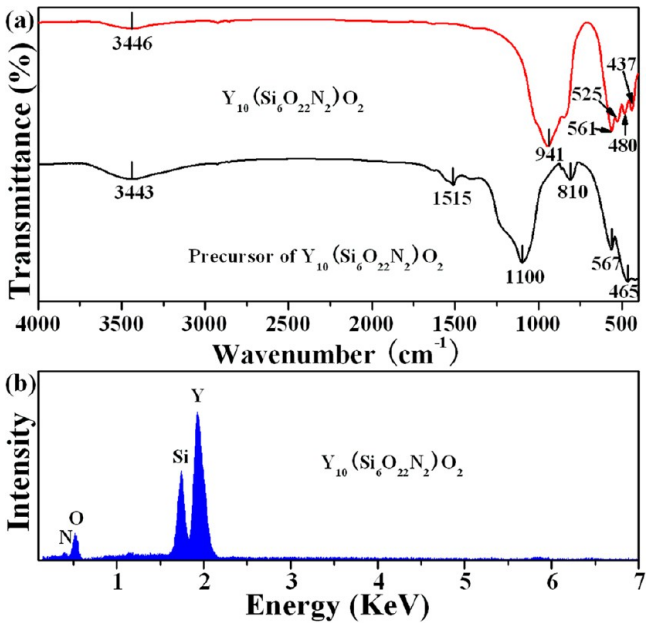

Figure 3. (a) FTIR spectra of the precursor of the $Y_{10}(Si_6O_{22}N_2)O_2$ and $Y_{10}(Si_6O_{22}N_2)O_2$ samples. (b) EDX spectrum of the $Y_{10}(Si_6O_{22}N_2)O_2$ host.

has a broad absorption band near 3443 cm^{-1}, which could be assigned to the stretching vibration of O–H bonds.[20] The absorption bands of the Si–O–Si (ν_{as}, 1100 cm^{-1}; ν_s, 810 cm^{-1}), Y–O (567 cm^{-1}), and Si–O (δ, 465 cm^{-1}) bonds (where ν_{as} = asymmetric stretching, ν_s = symmetric stretching, and δ = bending) are also observed.[21] The absorption band at 1515 cm^{-1} is due to the organic impurities that arise from the starting materials such as citric acid and PEG.[21c,22] The FTIR spectrum of the $Y_{10}(Si_6O_{22}N_2)O_2$ sample shows a profile different from that of its precursor. The absorption band of organic impurities disappears, and new absorption peaks located at 941, 525, and 480 cm^{-1} turn up. The Si–O(N) and Y–O(N) bonds in the $Y_{10}(Si_6O_{22}N_2)O_2$ compound may be responsible for those new peaks. The result proves that the chemical compositions of these two specimens are different. The composition of the precursor is a mixture of Y_2O_3 and SiO_2, as shown in Figure S1 in the SI. The final products were obtained by introducing a NH_3 flow at a temperature of 1200 °C, which can be expressed by the following reaction:

$$5Y_2O_3 + 6SiO_2 \xrightarrow{NH_3} Y_{10}(Si_6O_{22}N_2)O_2 \quad (1)$$

In addition, EDX analysis of the $Y_{10}(Si_6O_{22}N_2)O_2$ sample shown in Figure 3b also supplies competent evidence for formation of the desired samples.

TGA was carried out to determine the thermal stability and further confirm the composition of the as-prepared $Y_{10}(Si_6O_{22}N_2)O_2$ sample. Figure 4 shows the TGA curves of

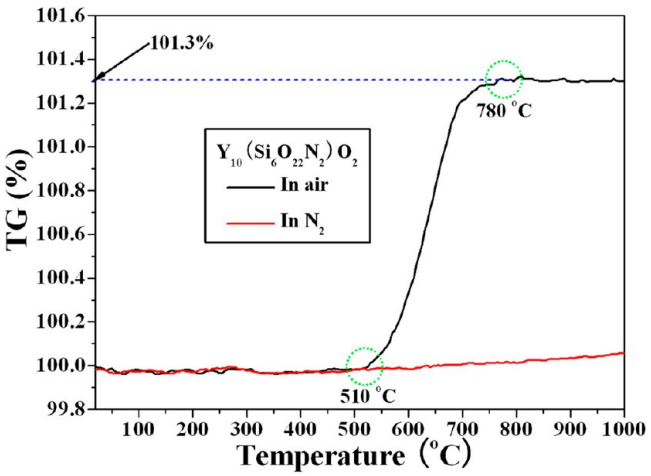

Figure 4. TGA curves of the $Y_{10}(Si_6O_{22}N_2)O_2$ sample in air and N_2 atmospheres.

the $Y_{10}(Si_6O_{22}N_2)O_2$ sample in air and N_2 atmospheres. From the TGA curve in air flow (black line), it is found that the weight of the product does not change significantly below 510 °C. From 510 to 780 °C, the weight of the sample increases gradually by about 1.3%. However, the weight of the sample remains almost unchanged at any temperature in nitrogen flow (red line). So, we can conclude that the powder has basically not been oxidized from room temperature to 510 °C without an inert atmosphere (N_2). However, the oxidation process became intensified as the temperature rose to 780 °C. The results reveal that the as-prepared $Y_{10}(Si_6O_{22}N_2)O_2$ sample has impressive thermal stability and antioxidation property. Because the valence states for the cations (Y^{3+} and Si^{4+}) in the $Y_{10}(Si_6O_{22}N_2)O_2$ host are unchanged, $Y_{10}(Si_6O_{22}N_2)O_2$ can finally be oxidized to $Y_{10}Si_6O_{27}$ (in form) in air at a temperature higher than 780 °C:

$$Y_{10}(Si_6O_{22}N_2)O_2 \xrightarrow{\text{oxidation}} Y_{10}Si_6O_{27}\ (\text{in form}) \quad (2)$$

So, the theoretical weight increment is 1.36% if $Y_{10}(Si_6O_{22}N_2)$-O_2 has been completely oxidized to $Y_{10}Si_6O_{27}$. The experimental value matches well with the theoretical value. Thus, we can further confirm that the composition of our sample is $Y_{10}(Si_6O_{22}N_2)O_2$.

dx.doi.org/10.1021/ic402916b | Inorg. Chem. 2014, 53, 2230–2239

3.2. PL Properties. *$Y_{10}(Si_6O_{22}N_2)O_2:Ce^{3+}$*. The excitation and emission spectra of the $Y_{10}(Si_6O_{22}N_2)O_2$:0.015Ce^{3+} phosphor are shown in Figure 5. Under 324 and 358 nm

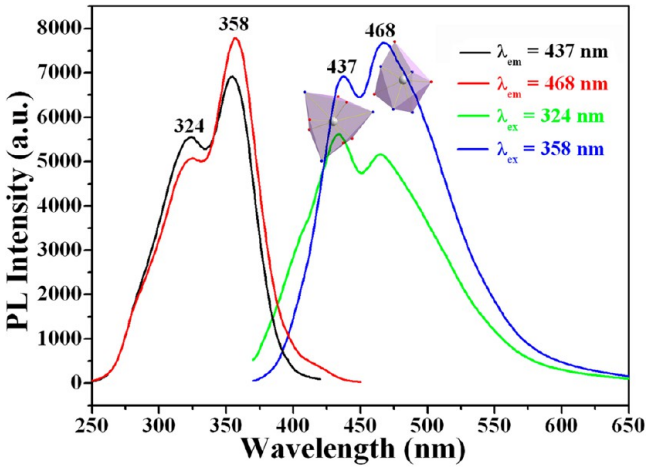

Figure 5. Excitation and emission spectra of the $Y_{10}(Si_6O_{22}N_2)$-O_2:0.015Ce^{3+} phosphor.

UV-light excitation, the $Y_{10}(Si_6O_{22}N_2)O_2$:0.015Ce^{3+} phosphor gives an asymmetric and splitting emission band ranging from 360 to 570 nm in wavelength due to the $5d^1 \rightarrow 4f^1$ transition of Ce^{3+}. The excitation spectra of the $Y_{10}(Si_6O_{22}N_2)O_2$:0.015Ce^{3+} phosphor monitored at 437 and 468 nm both consist of two separated bands in the region from 260 to 400 nm corresponding to the transitions from the ground state to the different crystal-field splitting levels of the 5d state for Ce^{3+} ions. Clearly, the intensity and shape of the excitation and emission spectra are different with different monitored bands. As we know, the emission spectrum for the phosphor doped with Ce^{3+} ions usually has doublet quality because of the spin−orbit splitting of the ground state ($^2F_{5/2}$ and $^2F_{7/2}$) with an energy difference of about 2000 cm^{-1}.[23] The energy difference between 437 and 468 nm is about 1516 cm^{-1}, which is far from 2000 cm^{-1}. So, the two emission bands cannot be ascribed to the splitting ground state of the single Ce^{3+} emission center. As discussed in section 3.1, Ce^{3+} ions can occupy two different crystallographic sites in the $Y_{10}(Si_6O_{22}N_2)O_2$ host. Therefore, the splitting bands located at 437 and 468 nm can be attributed to Ce^{3+} ions entering the 4f and 6h sites [denoted as Ce^{3+}(I) and Ce^{3+}(II)], respectively.[19] The selected emission spectra of $Y_{10}(Si_6O_{22}N_2)O_2$:*x*Ce^{3+} with different concentrations of Ce^{3+} (*x*) are displayed in Figure S2 in the SI. Clearly, the doped Ce^{3+} ions prefer to occupy the 4f site in the $Y_{10}(Si_6O_{22}N_2)O_2$ host at low doping concentrations. Figure S3 in the SI shows the relationship between the emission intensity of Ce^{3+} ions and *x* in the $Y_{10}(Si_6O_{22}N_2)O_2$:*x*Ce^{3+} system. Obviously, the optimum doping concentration of Ce^{3+} in the $Y_{10}(Si_6O_{22}N_2)O_2$ host is 1.5 mol % of Y^{3+}. The emission intensity decreases with a further increase in the value of *x* because of the concentration quenching effect.[24]

$Y_{10}(Si_6O_{22}N_2)O_2:Mn^{2+}$. The transition-metal ion Mn^{2+} has a bare $3d^5$ electronic configuration. So, the band position of the Mn^{2+} emission spectrum, which consists of a broad band [corresponding to the $^4T_1(^4G) \rightarrow {}^6A_1(6S)$ transition], depends strongly on the crystal-field strength of the host lattices. If the crystal field around Mn^{2+} is weak, the splitting of the excited 3d energy levels will be small, resulting in Mn^{2+} emission with higher energy; otherwise, the Mn^{2+} ions can emit light with low energy.[25] So, one can realize red emission if the right host has been chosen.

The excitation and emission spectra of the $Y_{10}(Si_6O_{22}N_2)$-O_2:0.07Mn^{2+} sample are presented in Figure 6. We can observe

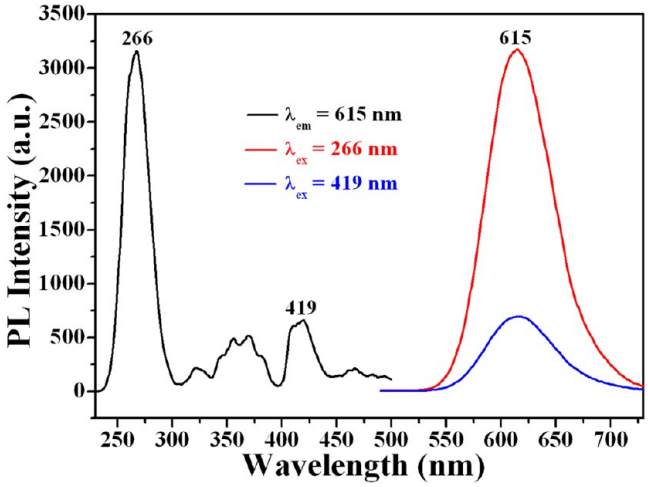

Figure 6. Excitation and emission spectra of $Y_{10}(Si_6O_{22}N_2)$-O_2:0.07Mn^{2+} phosphor.

that the excitation spectrum includes a very strong band centered at 266 nm and several weak bands from 300 to 500 nm. The former can be attributed to the charge-transfer transition of Mn^{2+} ions, and the latter can be attributed to the forbidden d−d transitions of Mn^{2+}.[26] Under 266 nm UV-light excitation, the $Y_{10}(Si_6O_{22}N_2)O_2$:0.07Mn^{2+} phosphor gives a symmetrical and broad emission band centered at 615 nm, which can be ascribed to the spin-forbidden $^4T_1(^4G) \rightarrow {}^6A_1(6S)$ transition of Mn^{2+} ions. This observation is consistent with the speculation that the Mn^{2+} ions just occupied one crystallographic site (4f site) in the $Y_{10}(Si_6O_{22}N_2)O_2$ host proposed in section 3.1. In addition, we also noticed that the emission band of Mn^{2+} ions in the $Y_{10}(Si_6O_{22}N_2)O_2$:*y*Mn^{2+} system gradually shifts to the long-wavelength direction with increasing Mn^{2+} concentration. For radii of Mn^{2+} ions smaller than those of Y^{3+} ions, the crystal lattice of $Y_{10}(Si_6O_{22}N_2)O_2$ will shrink after doping of a high Mn^{2+} concentration into the host to replace Y^{3+}. Then, the crystal-field strength surrounding Mn^{2+} ions becomes stronger, which further results in a larger crystal-field splitting of the Mn^{2+} 3d energy levels. As mentioned above, the strong crystal-field strength could cause Mn^{2+} to give a longer-wavelength emission. In addition, we have also investigated the concentration quenching effect of the $Y_{10}(Si_6O_{22}N_2)O_2$:*y*Mn^{2+} sample with a change in the content of Mn^{2+} ions. Figure S4 in the SI shows the emission intensity of Mn^{2+} as a function of its doping concentration (*y*). Evidently, the optimum doping concentration of Mn^{2+} is *y* = 0.06.

$Y_{10}(Si_6O_{22}N_2)O_2:Ce^{3+},Mn^{2+}$. A comparison of the excitation spectrum for $Y_{10}(Si_6O_{22}N_2)O_2$:0.07Mn^{2+} and the emission spectra for $Y_{10}(Si_6O_{22}N_2)O_2$:0.015Ce^{3+} is shown in Figure S5 in the SI. The result reveals that there is great spectral overlap between the emission band of Ce^{3+}(I) centered at 437 band and the Mn^{2+} excitation transitions of $^6A_1(6S) \rightarrow {}^4A_1(^4G)$, $^4E(^4G)$.[27] Accordingly, the occurrence of efficient resonance-type energy transfer from Ce^{3+} to Mn^{2+} in the $Y_{10}(Si_6O_{22}N_2)O_2$ host is possible. Figure 7a gives excitation spectra of the

dx.doi.org/10.1021/ic402916b | Inorg. Chem. 2014, 53, 2230−2239

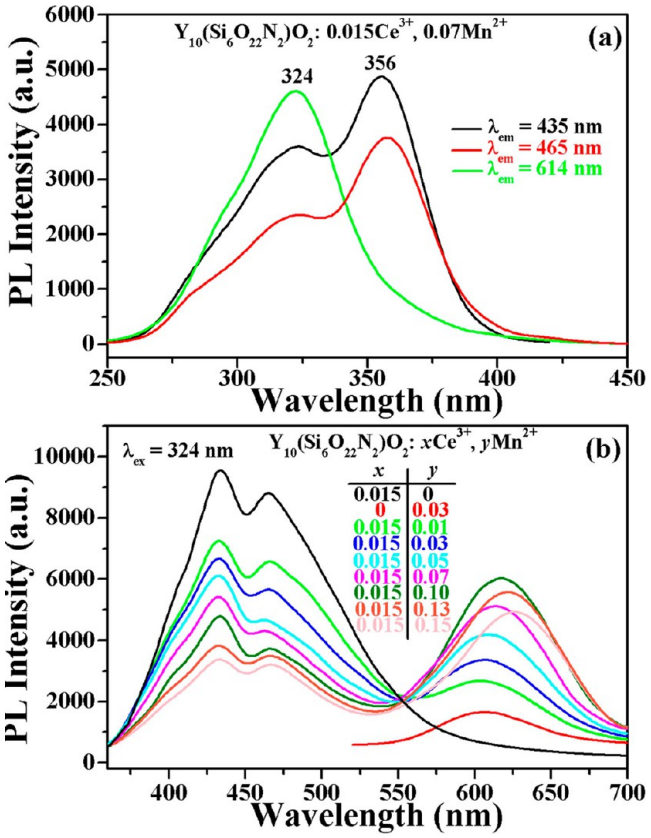

Figure 7. Excitation spectra for the $Y_{10}(Si_6O_{22}N_2)O_2$:0.015Ce^{3+},0.07Mn^{2+} sample (a) and emission spectra of the $Y_{10}(Si_6O_{22}N_2)O_2$:0.015Ce^{3+},yMn^{2+} samples with different Mn^{2+} doping concentrations (b).

$Y_{10}(Si_6O_{22}N_2)O_2$:0.015Ce^{3+},0.07Mn^{2+} phosphor monitored with typical emissions of Ce^{3+}(I), Ce^{3+}(II), and Mn^{2+} ions, respectively. The profiles of the excitation spectra for the $Y_{10}(Si_6O_{22}N_2)O_2$:0.015Ce^{3+},0.07Mn^{2+} phosphor monitored with the emission of Ce^{3+} ions are almost identical with those of the $Y_{10}(Si_6O_{22}N_2)O_2$:0.015Ce^{3+} sample. However, a comparison between the excitation spectrum of the $Y_{10}(Si_6O_{22}N_2)O_2$:0.015Ce^{3+},0.07Mn^{2+} phosphor monitored with the typical emission band of Mn^{2+} ions (614 nm) and that of the $Y_{10}(Si_6O_{22}N_2)O_2$:0.015Ce^{3+} phosphor monitored with the emission band of Ce^{3+} ions indicates that Mn^{2+} ions in the $Y_{10}(Si_6O_{22}N_2)O_2$:0.015Ce^{3+},0.07Mn^{2+} phosphor are essentially excited by the absorption band of Ce^{3+} ions through the energy-transfer process. The short UV wavelength (324 nm) of the absorption band for the $Y_{10}(Si_6O_{22}N_2)O_2$:Ce^{3+} phosphor selectively excites the Ce^{3+}(I) center, while the long UV wavelength (358 nm) prefers to excite the Ce^{3+}(II) center. According to the profile of the excitation spectrum for the $Y_{10}(Si_6O_{22}N_2)O_2$:0.015Ce^{3+},0.07Mn^{2+} phosphor monitored with Mn^{2+} emission (green line in Figure 7a), we can speculate that Ce^{3+}(I) contributed more to the emission of Mn^{2+} in the $Y_{10}(Si_6O_{22}N_2)O_2$:Ce^{3+},Mn^{2+} phosphor.

Figure 7b displays emission spectra for the $Y_{10}(Si_6O_{22}N_2)O_2$:0.015Ce^{3+},yMn^{2+} samples under excitation of 324 nm UV light. All of the emission spectra are composed of a splitting blue band (Ce^{3+} emission) and a reddish-orange band (Mn^{2+} emission), which indicate that Ce^{3+} ions have successfully transferred their absorbed energy to Mn^{2+} ions. In the $Y_{10}(Si_6O_{22}N_2)O_2$:0.015Ce^{3+},yMn^{2+} samples, the emission intensity of Ce^{3+} decreased and that for Mn^{2+} increased with increasing Mn^{2+} concentration. The relative integrated emission intensities of Ce^{3+} and Mn^{2+} ions are present in Figure S6 in the SI. The emission intensity of Mn^{2+} reaches its maximum value at y = 0.10 in the $Y_{10}(Si_6O_{22}N_2)O_2$:0.015Ce^{3+},yMn^{2+} system. In general, the expression $\eta = 1 - I_S/I_{S0}$ (η is the energy-transfer efficiency, and I_S and I_{S0} are the luminescence intensities of the sensitizer with and without the activator present) can be used to estimate the energy-transfer efficiency from the sensitizer to the activator.[28] According to the relative emission intensity of Ce^{3+} ions shown in Figure S6 in the SI, we can deduce that the energy-transfer efficiency (η) increases with the addition of the content of Mn^{2+} ions. The controllable emission color is an attractive feature that can be obtained in most energy-transfer systems. In our study, we investigated the adjustment of the emission color for the $Y_{10}(Si_6O_{22}N_2)O_2$:0.015Ce^{3+},yMn^{2+} samples with a change in the Mn^{2+} doping concentration. Figure 8 depicts the CIE chromaticity coordinates of the $Y_{10}(Si_6O_{22}N_2)O_2$:0.015Ce^{3+},yMn^{2+} samples. By codoping Mn^{2+} ions into the $Y_{10}(Si_6O_{22}N_2)O_2$:0.015Ce^{3+} phosphor, the emission color can be adjusted from blue (x = 0.1739, y = 0.187) to reddish-orange (x = 0.4268, y = 0.3581) with increasing Mn^{2+} concentration. Although most of the current UV chips used in W-LEDs can only have excitation ability in the wavelength of 380−420 nm, more short UV-emitting chips (300−380 nm) may be available in the future with the development of a semiconductor chip.

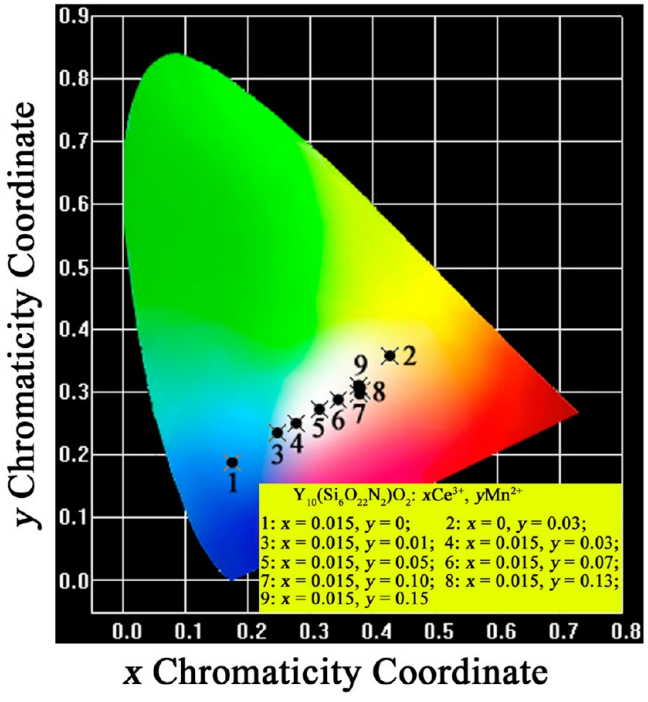

Figure 8. CIE chromaticity coordinates of the $Y_{10}(Si_6O_{22}N_2)O_2$:$x$$Ce^{3+}$,y$Mn^{2+}$ samples with different Ce^{3+} and Mn^{2+} doping concentrations.

Figure 9 provides the fluorescence decay curves of Ce^{3+}(I) and Ce^{3+}(II) in the $Y_{10}(Si_6O_{22}N_2)O_2$:0.015Ce^{3+},yMn^{2+} samples with different Mn^{2+} concentrations under excitation of 324 nm UV light. The different decay behaviors for Ce^{3+}(I) and Ce^{3+}(II) support the fact that the splitting emission band originates from two separate Ce^{3+} centers.

dx.doi.org/10.1021/ic402916b | Inorg. Chem. 2014, 53, 2230−2239

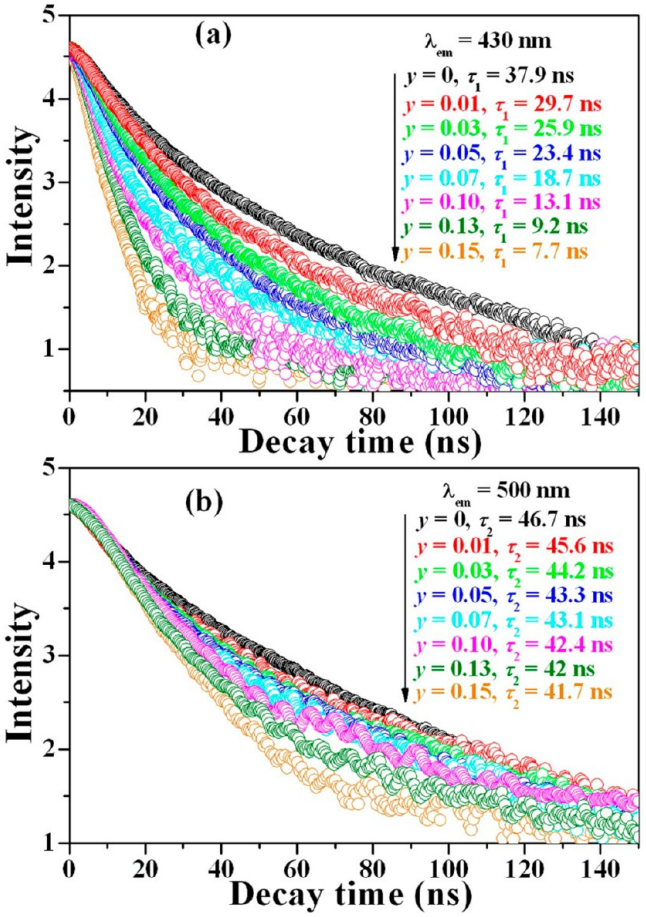

Figure 9. Decay curves for luminescence of Ce^{3+} in the $Y_{10}(Si_6O_{22}N_2)O_2$:0.015Ce^{3+},yMn^{2+} samples with different Mn^{2+} doping concentrations (λ_{ex} = 324 nm).

$$I(t) = A_1 \exp(-t/\tau_1) + A_2 \exp(-t/\tau_2) \quad (3)$$

$$\tau = (A_1\tau_1^2 + A_2\tau_2^2)/(A_1\tau_1 + A_2\tau_2) \quad (4)$$

The decay curves of Ce^{3+}(I) and Ce^{3+}(II) in $Y_{10}(Si_6O_{22}N_2)O_2$:0.015Ce^{3+},yMn^{2+} phosphors can both be fitted by eq 3, and the lifetime can be calculated by eq 4.[29] In the above equations, $I(t)$ represents the luminescence intensity at a time t, A_1 and A_2 are constants, τ_1 and τ_2 are rapid and slow lifetimes for exponential components, respectively, t is the time, and τ is the average decay time. According to eqs 3 and 4, the lifetimes for Ce^{3+}(I) and Ce^{3+}(II) have been calculated and are listed in Figure 9a,b. Distinctly, the lifetimes for both Ce^{3+}(I) and Ce^{3+}(II) are shortened by increasing the content of Mn^{2+} ions, which is convincing evidence for energy transfer from Ce^{3+} to Mn^{2+} ions in the $Y_{10}(Si_6O_{22}N_2)O_2$ host. However, a decrease of the lifetime for Ce^{3+}(I) is much more conspicuous than that of Ce^{3+}(II). Hence, we can guess that energy transfer from Ce^{3+}(I) to Mn^{2+} is more efficient. Besides the emission intensity of the sensitizer, the energy-transfer efficiency from Ce^{3+} to Mn^{2+} can also be estimated by the lifetimes of the sensitizer:[30]

$$\eta = 1 - \frac{\tau}{\tau_0} \quad (5)$$

where τ_0 and τ are the lifetimes of the sensitizer without and with the activator, respectively. Figure 10 shows the dependence of the energy-transfer efficiency η_1 [Ce^{3+}(I) → Mn^{2+}] and η_2 [Ce^{3+}(II) → Mn^{2+}] on the Mn^{2+} doping concentration. When y = 0.15, the energy-transfer efficiencies η_1 and η_2 are 80% and 10%, respectively. The result can be supported by Figure S5 in the SI, which can be interpreted by larger spectral overlap between Ce^{3+}(I) emission and Mn^{2+} excitation than that between Ce^{3+}(II) and Mn^{2+}. That is because the energy-transfer probability (PSA) from a sensitizer to an acceptor is proportional to the spectral overlap between the emission band of the sensitizer and the excitation band of the acceptor.[31]

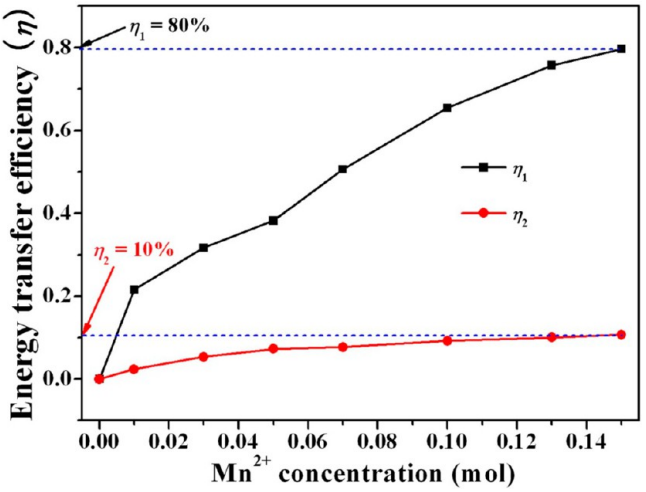

Figure 10. Dependence of the energy-transfer efficiencies η_1 and η_2 on the Mn^{2+} doping concentration (λ_{ex} = 324 nm).

3.3. Temperature Quenching. As we know, phosphors applied to LEDs must have stable PL properties at an operation temperature of about 150 °C over the long term.[32] So, investigation of the thermal stability for the samples must be carried out when preparing phosphors for LEDs. The emission intensity and chromaticity coordinates are the two most important qualities that should be taken into account. Figure 11a shows the emission spectra of the $Y_{10}(Si_6O_{22}N_2)O_2$:0.015Ce^{3+},0.03Mn^{2+} phosphor with respect to the temperature. As shown in Figure 11b, the integrated emission intensity drops with an increase in the temperature. The emission intensity of the $Y_{10}(Si_6O_{22}N_2)O_2$:0.015Ce^{3+},0.03Mn^{2+} sample remains at about 74% of the initial emission intensity at a temperature of 423 K (150 °C). With increasing temperature, the emission band position for Ce^{3+} ions stays unchanged, whereas the emission band of Mn^{2+} ions shows a blue shift. A similar phenomenon has been found and studied in other phosphors doped with Mn^{2+} ions.[33] The CIE chromaticity coordinates for the $Y_{10}(Si_6O_{22}N_2)O_2$:0.015Ce^{3+},0.03Mn^{2+} sample at different temperature are shown in Figure S7 in the SI. All of the results prove that $Y_{10}(Si_6O_{22}N_2)O_2$:Ce^{3+},Mn^{2+} phosphors have good thermal stability and color stability under high-temperature conditions. Additionally, the activation energy ΔE can be calculated by the following expression:[34]

$$I_T = I_0\left[1 + c\exp\left(-\frac{\Delta E}{kT}\right)\right]^{-1} \quad (6)$$

in which I_0 is the initial emission intensity, I_T is the emission intensity at different temperatures, c is a constant for a certain host, k is the Boltzmann constant (8.629×10^{-5} eV/K), and T is the temperature. In the inset of Figure 11b, the relationship between $\ln[(I_0/I_T) - 1]$ and $1/kT$ for the $Y_{10}(Si_6O_{22}N_2)$-

dx.doi.org/10.1021/ic402916b | Inorg. Chem. 2014, 53, 2230−2239

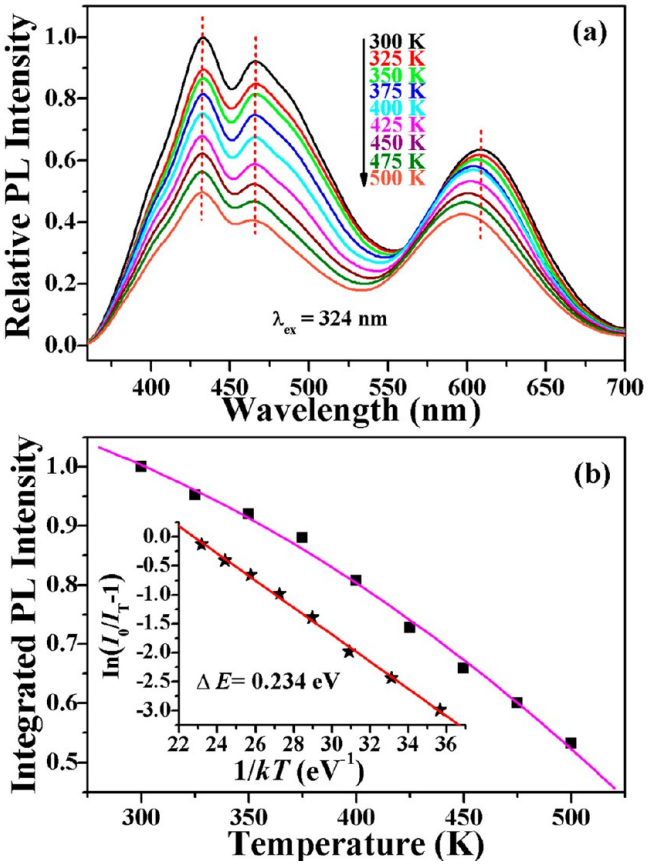

Figure 11. Temperature-dependent emission spectra (a) and plots of $\ln[(I_0/I_T) - 1]$ versus $1/kT$ (b) for the $Y_{10}(Si_6O_{22}N_2)O_2$: $0.015Ce^{3+}$, $0.03Mn^{2+}$ sample.

O_2:$0.015Ce^{3+}$,$0.03Mn^{2+}$ sample is presented. On the basis of eq 6, ΔE of the $Y_{10}(Si_6O_{22}N_2)O_2$:$0.015Ce^{3+}$,$0.03Mn^{2+}$ sample was estimated to be 0.234 eV. This result further confirms the good thermal stability of as-prepared $Y_{10}(Si_6O_{22}N_2)O_2$:Ce^{3+},Mn^{2+} phosphors.

3.4. CL Properties. Under low-voltage electron-beam excitation, the CL properties and the degradation property for as-prepared $Y_{10}(Si_6O_{22}N_2)O_2$:Ce^{3+},Mn^{2+} phosphors have been investigated in detail. The typical CL spectra for $Y_{10}(Si_6O_{22}N_2)O_2$:$0.015Ce^{3+}$, $Y_{10}(Si_6O_{22}N_2)O_2$:$0.07Mn^{2+}$, and $Y_{10}(Si_6O_{22}N_2)O_2$:$0.015Ce^{3+}$,$0.03Mn^{2+}$ phosphors along with their matching digital luminescence photographs are displayed in Figure 12. Compared with their PL properties, the CL spectra have no significant change. However, the CL emission band for $Y_{10}(Si_6O_{22}N_2)O_2$:$0.015Ce^{3+}$ is the combination of their PL spectra excited by 324 and 358 nm UV light. This can be explained by the fact that the electron beam has fairly high energy and it cannot selectively excite a specific luminescent center [Ce^{3+}(I) or Ce^{3+}(II)]. Moreover, the emission intensity for Mn^{2+} in the $Y_{10}(Si_6O_{22}N_2)O_2$:$0.015Ce^{3+}$,$0.03Mn^{2+}$ phosphor increased with the respect of that for Ce^{3+} ions. This can be attributed to different excitation sources.[35] Additionally, energy transfer from Ce^{3+} to Mn^{2+} in the $Y_{10}(Si_6O_{22}N_2)$-O_2:Ce^{3+},Mn^{2+} system has also been noticed in their CL spectra. With the same doping concentration, the emission intensity for Mn^{2+} ions increases distinctly by introducing Ce^{3+} ions into $Y_{10}(Si_6O_{22}N_2)O_2$:Mn^{2+} samples. As expected, the tunable CL color can also be achieved. The emission color of the $Y_{10}(Si_6O_{22}N_2)O_2$:$0.015Ce^{3+}$,$0.03Mn^{2+}$ phosphor is gray to the

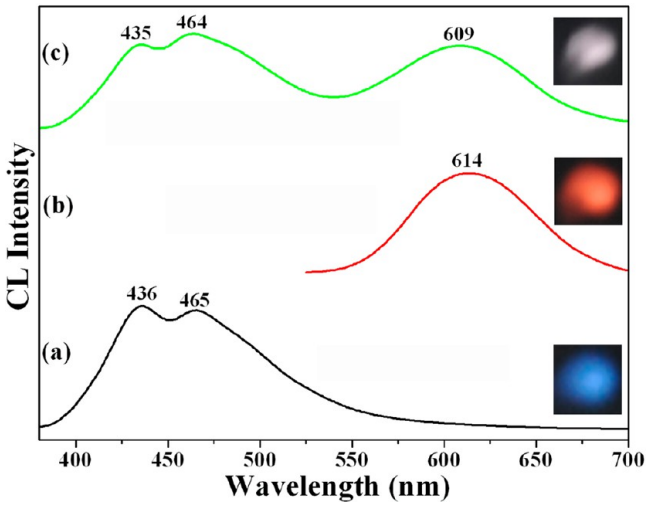

Figure 12. CL spectra for $Y_{10}(Si_6O_{22}N_2)O_2$:$0.015Ce^{3+}$ (a), $Y_{10}(Si_6O_{22}N_2)O_2$:$0.07Mn^{2+}$ (b), and $Y_{10}(Si_6O_{22}N_2)$-O_2:$0.015Ce^{3+}$,$0.05Mn^{2+}$ (c). The insets are their corresponding digital luminescence photographs under low-voltage electron-beam excitation.

naked eyes with the CIE chromaticity coordinates of (x = 0.3278, y = 0.2814). Moreover, the maximum current density for the $Y_{10}(Si_6O_{22}N_2)O_2$:Ce^{3+},Mn^{2+} phosphor is 41 $\mu A/cm^2$ with the electron voltage fixed at 5.0 kV. According to the literature,[36] the phosphors that have current densities ranging from 10 to 100 $\mu A/cm^2$ under excitation of lower electron voltages ($\lesssim$5 kV) can serve as the FED phosphor. So, the $Y_{10}(Si_6O_{22}N_2)O_2$:Ce^{3+},Mn^{2+} phosphor can be a good candidate material for FEDs.

We also investigated the degradation behavior of CL for the $Y_{10}(Si_6O_{22}N_2)O_2$:$0.015Ce^{3+}$ sample under low-voltage electron-beam excitation. Figure 13 shows the dependence of the relative CL intensity of Y_2SiO_5:Ce^{3+} (commercial) and $Y_{10}(Si_6O_{22}N_2)O_2$:$0.015Ce^{3+}$ on the radiation time (0−120 min) under electron-beam excitation. The CL intensities for both Y_2SiO_5:Ce^{3+} and $Y_{10}(Si_6O_{22}N_2)O_2$:$0.015Ce^{3+}$ phosphors decrease gradually with prolonged electron bombardment time.

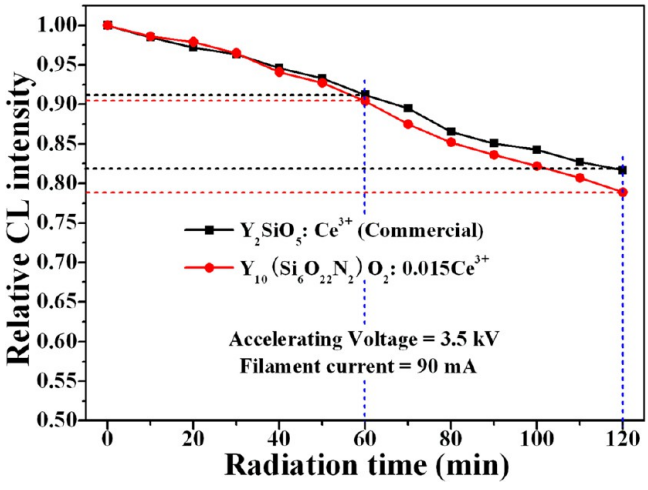

Figure 13. Dependence of the relative CL intensity of Y_2SiO_5: Ce^{3+} (commercial) and $Y_{10}(Si_6O_{22}N_2)O_2$:$0.015Ce^{3+}$ on the radiation time under low-voltage electron-beam excitation (accelerating voltage = 3.5 kV; filament current = 90 mA).

dx.doi.org/10.1021/ic402916b | Inorg. Chem. 2014, 53, 2230−2239

The CL intensity of the Y_2SiO_5: Ce^{3+} phosphor falls to 91 and 82%, and that for the $Y_{10}(Si_6O_{22}N_2)O_2$:0.015Ce^{3+} sample drops to 90 and 79% of their initial values after continuous electron radiation for 60 and 120 min, respectively. So, the $Y_{10}(Si_6O_{22}N_2)O_2$:0.015Ce^{3+} sample has almost the same stability as the commercial Y_2SiO_5:Ce^{3+} phosphor. The more stable products may be obtained by improving the synthesis conditions. The accumulation of carbon at the surface of the samples during electron bombardment may be responsible for degradation of the CL intensity.[37] Some permanent damage to the structure of $Y_{10}(Si_6O_{22}N_2)O_2$:0.015Ce^{3+} after electron bombardment for a certain time may be another reason to the decrease of the CL intensity. Although the emission intensity changes a lot, the emission color for these two phosphors is nearly invariable under continuous electron radiation for 2 h. The investigation on the degradation of CL for the $Y_{10}(Si_6O_{22}N_2)O_2$:0.015Ce^{3+} phosphor indicates that the as-prepared samples have stable CL intensity and CIE color coordinates under electron bombardment.

4. CONCLUSION

In summary, we presented a convenient, economical, and energy-saving soft-chemical method to prepare the $Y_{10}(Si_6O_{22}N_2)O_2$ and $Y_{10}(Si_6O_{22}N_2)O_2$:Ce^{3+},Mn^{2+} samples for the first time. The crystal structure, phase purity, crystallinity, morphology, and PL and CL properties of as-prepared phosphors were well discussed. For monodoped $Y_{10}(Si_6O_{22}N_2)O_2$ samples, Ce^{3+} ions can occupy both the 4f and 6h sites and its emission spectrum shows a splitting band, while the Mn^{2+} ions can only hold 4f sites and exhibit reddish-orange emission because of the $^4T_1(^4G) \rightarrow {}^6A_1(6S)$ transition. Energy transfer from Ce^{3+}(I) to Mn^{2+} is more efficient than that from Ce^{3+}(II) to Mn^{2+}, which can be attributed to the larger spectral overlap between Ce^{3+}(I) emission and Mn^{2+} excitation than that between Ce^{3+}(II) and Mn^{2+}. Tunable emission from blue to reddish-orange can be realized by energy transfer and a change in the doping concentrations of the activators under UV-light and low-voltage electron-beam excitation. The investigation of the temperature-dependent PL properties for the $Y_{10}(Si_6O_{22}N_2)O_2$:0.015Ce^{3+},0.05Mn^{2+} phosphor demonstrates that our samples have good thermal stability. The study of the degradation property of CL for $Y_{10}(Si_6O_{22}N_2)O_2$:0.015Ce^{3+} under continuous electron bombardment proves that the as-synthesized phosphors can serve as the phosphor applied in FEDs. All in all, because of their good luminescence properties, structure stability, low raw-material cost, and energy-saving preparation method, the $Y_{10}(Si_6O_{22}N_2)O_2$:Ce^{3+},Mn^{2+} phosphors have promising applications in W-LEDs and FEDs.

■ ASSOCIATED CONTENT

Supporting Information

Structural parameters for $Y_{10}(Si_6O_{22}N_2)O_2$ determined by Rietveld refinement of powder XRD data at room temperature (Table S1), XRD pattern for a precursor of the $Y_{10}(Si_6O_{22}N_2)O_2$ sample (Figure S1), various emission spectra of the $Y_{10}(Si_6O_{22}N_2)O_2$: $x$$Ce^{3+}$ phosphors with different Ce^{3+} doping concentrations (Figure S2), emission intensity of Ce^{3+} as a function of its doping concentration (x) in the $Y_{10}(Si_6O_{22}N_2)O_2$: $x$$Ce^{3+}$ sample (Figure S3), emission intensity of Mn^{2+} as a function of its doping concentration (y) in the $Y_{10}(Si_6O_{22}N_2)O_2$: $y$$Mn^{2+}$ sample (Figure S4), spectral overlap between the emission band of $Y_{10}(Si_6O_{22}N_2)O_2$: 0.015Ce^{3+} and the excitation spectra of $Y_{10}(Si_6O_{22}N_2)O_2$: 0.07Mn^{2+} (Figure S5), relative emission intensity of Ce^{3+} and Mn^{2+} in $Y_{10}(Si_6O_{22}N_2)O_2$: 0.015Ce^{3+}, $y$$Mn^{2+}$ samples with different Mn^{2+} doping concentrations (Figure S6), and CIE chromaticity coordinates for the $Y_{10}(Si_6O_{22}N_2)O_2$: 0.015Ce^{3+}, 0.03Mn^{2+} sample at different temperatures (Figure S7). This material is available free of charge via the Internet at http://pubs.acs.org.

■ AUTHOR INFORMATION

Corresponding Author

*E-mail: jlin@ciac.ac.cn.

Notes

The authors declare no competing financial interest.

■ ACKNOWLEDGMENTS

This project is financially supported by the National Natural Science Foundation of China (NSFC Grants 51332008, 51172227, and 21221061), National Basic Research Program of China (Grants 2010CB327704 and 2014CB643803), and Joint Funds of the National Natural Science Foundation of China (Grant U13012038).

■ REFERENCES

(1) (a) Jing, H.; Guo, C.; Zhang, G.; Su, X.; Yang, Z.; Jeong, J. H. *J. Mater. Chem.* **2012**, *22*, 13612−13618. (b) Su, S.; Liu, W.; Duan, R.; Cao, L.; Su, G.; Zhao, C. *J. Alloys Compd.* **2013**, *575*, 309−313. (c) Xia, Z.; Zhuang, J.; Liao, L. *Inorg. Chem.* **2012**, *51*, 7202−7209. (d) Lozano, G.; Louwers, D. J.; Rodríguez, S. R. K.; Murai, S.; Jansen, O. T. A.; Verschuuren, M. A.; Rivas, J. G. *Light: Sci. Appl.* **2013**, *2*, e66. (e) Zhang, Z.; Wang, J.; Zhang, M.; Zhang, Q.; Su, Q. *Appl. Phys. B: Lasers Opt.* **2008**, *91*, 529−537.

(2) (a) Liu, Y.; Zhang, X.; Hao, Z.; Wang, X.; Zhang, J. *Chem. Commun.* **2011**, *47*, 10677−10679. (b) Li, X.; Budai, J. D.; Liu, F.; Howe, J. Y.; Zhang, J.; Wang, X.-J.; Gu, Z.; Sun, C.; Meltzer, R. S.; Pan, Z. *Light: Sci. Appl.* **2013**, *2*, e50. (c) Wu, Y.-C.; Chen, Y.-C.; Wang, D.-Y.; Lee, C.-S.; Sun, C.-C.; Chen, T.-M. *J. Mater. Chem.* **2011**, *21*, 15163−15166.

(3) (a) Hsu, C.-H.; Das, S.; Lu, C.-H. *J. Electrochem. Soc.* **2012**, *159*, J193−J199. (b) Wu, L.; Zhang, Y.; Gui, M.; Lu, P.; Zhao, L.; Tian, S.; Kong, Y.; Xu, J. *J. Mater. Chem.* **2012**, *22*, 6463−6470. (c) Huang, C. H.; Chen, T. M. *J. Phys. Chem. C* **2011**, *115*, 2349−2355.

(4) (a) Do, Y. R.; Kim, Y.-C.; Shin, N.; Sohn, K.-S. *Electrochem. Solid-State Lett.* **2005**, *8*, H43−H45. (b) Liu, C.; Zhang, S.; Liu, Z.; Liang, H.; Sun, S.; Tao, Y. *J. Mater. Chem. C* **2013**, *1*, 1305−1308.

(5) Liu, T.-C.; Kominami, H.; Greer, H. F.; Zhou, W.; Nakanishi, Y.; Liu, R.-S. *Chem. Mater.* **2012**, *24*, 3486−3492.

(6) (a) Zhang, M.; Wang, X.; Ding, H.; Li, H.; Pan, L.; Sun, Z. *Int. J. Appl. Ceram. Technol.* **2011**, *8*, 752−758. (b) Li, H. L.; Wang, Z. L.; Xu, S. J.; Hao, J. H. *J. Electrochem. Soc.* **2009**, *156*, J112−J116. (c) Liu, X.; Liu, Y.; Yan, D.; Zhu, H.; Liu, C.; Xu, C.; Liu, Y.; Wang, X. *J. Mater. Chem.* **2012**, *22*, 16839−16843.

(7) (a) Sobczak-Kupiec, A.; Wzorek, Z.; Kijkowska, R.; Kowalski, Z. *Bull. Mater. Sci.* **2013**, *36*, 755−764. (b) Zhang, C.; Li, C.; Huang, S.; Hou, Z.; Cheng, Z.; Yang, P.; Peng, C.; Lin, J. *Biomaterials* **2010**, *31*, 3374−3383. (c) Yoo, H. S.; Vaidyanathan, S.; Kim, S. W.; Jeon, D. Y. *Opt. Mater.* **2009**, *31*, 1555−1558. (d) Shang, M.; Geng, D.; Yang, D.; Kang, X.; Zhang, Y.; Lin, J. *Inorg. Chem.* **2013**, *52*, 3102−3112.

(8) Su, Q.; Lin, J.; Li, B. *J. Alloys Compd.* **1995**, *225*, 120−123.

(9) (a) Shang, M.; Li, G.; Geng, D.; Yang, D.; Kang, X.; Zhang, Y.; Lian, H.; Lin, J. *J. Phys. Chem. C* **2012**, *116*, 10222−10231. (b) Shang, M.; Geng, D.; Zhang, Y.; Li, G.; Yang, D.; Kang, X.; Lin, J. *J. Mater. Chem.* **2012**, *22*, 19094−19104. (c) Wang, X. Q.; Han, X. M.; Zhen, C. M. *J. Nanosci. Nanotechnol.* **2011**, *11*, 9714−9716. (d) Lin, J.; Su, Q. *J. Alloys Compd.* **1994**, *210*, 159−163.

(10) (a) Yang, H.; Liu, Y.; Ye, S.; Qiu, J. *Chem. Phys. Lett.* **2008**, *451*, 218−221. (b) Chen, W.-T.; Sheu, H.-S.; Liu, R.-S.; Attfield, J. P. *J. Am.*

Chem. Soc. **2012**, *134*, 8022−8025. (c) Wang, X.-M.; Wang, C.-H.; Wu, M. M.; Wang, Y. X.; Jing, X.-P. *J. Mater. Chem.* **2012**, *22*, 3388−3394.
(11) (a) Park, W. B.; Song, Y.; Pyo, M.; Sohn, K.-S. *Opt. Lett.* **2013**, *38*, 1739−1741. (b) Ryu, J. H.; Won, H. S.; Park, Y.-G.; Kim, S. H.; Song, W. Y.; Suzuki, H.; Yoon, C. *Appl. Phys. A: Mater. Sci. Process.* **2009**, *95*, 747−752. (c) Kimura, N.; Sakuma, K.; Hirafune, S.; Asano, K.; Hirosaki, N.; Xie, R.-J. *Appl. Phys. Lett.* **2007**, *90*, 051109. (d) Li, Y. Q.; Hirosaki, N.; Xie, R. J.; Takeda, T.; Mitomo, M. *Chem. Mater.* **2008**, *20*, 6704−6714.
(12) (a) Van Krevel, J. W. H.; Hintzen, H. T.; Metselaar, R. *Mater. Res. Bull.* **2000**, *35*, 747−754. (b) Kurushima, T.; Gundiah, G.; Shimomura, Y.; Mikami, M.; Kijima, N.; Cheetham, A. K. *J. Electrochem. Soc.* **2010**, *157*, J64−J68.
(13) (a) Van Krevel, J. W. H.; Hintzen, H. T.; Metselaar, R.; Meijerink, A. *J. Alloys Compd.* **1998**, *268*, 272−277. (b) Menke, Y.; Hampshire, S.; Falk, L. K. L. *J. Am. Ceram. Soc.* **2007**, *90*, 1566−1573. (c) Inoue, K.; Hirosaki, N.; Xie, R.-J.; Takeda, T. *J. Phys. Chem. C* **2009**, *113*, 9392−9397.
(14) (a) Li, Y. Q.; Fang, C. M.; de With, G.; Hintzen, H. T. *J. Solid State Chem.* **2004**, *177*, 4687−4694. (b) Duan, C. J.; Delsing, A. C. A.; Hintzen, H. T. *J. Lumin.* **2009**, *129*, 645−649. (c) Chen, C.; Chen, W.; Rainwater, B.; Liu, L.; Zhang, H.; Liu, Y.; Guo, X.; Zhou, J.; Xie, E. *Opt. Lett.* **2011**, *33*, 1585−1590.
(15) Thomas, S.; Oró-Solé, J.; Glorieux, B.; Jubera, V.; Buissette, V.; Le Mercier, T.; Garcia, A.; Fuertes, A. *J. Mater. Chem.* **2012**, *22*, 23913−23920.
(16) Larson, A. C.; Von Dreele, R. B. *General Structure Analysis System (GSAS)*; Los Alamos National Laboratory Report LAUR 86-748; Los Alamos National Laboratory: Los Alamos, NM, 1994.
(17) Lammers, M. J. J.; Blasse, G. *J. Electrochem. Soc.* **1987**, *134*, 2068−2072.
(18) Shannon, R. D. *Acta Crystallogr.* **1976**, *A32*, 751−767.
(19) Li, G.; Zhang, Y.; Geng, D.; Shang, M.; Peng, C.; Cheng, Z.; Lin, J. *ACS Appl. Mater. Interfaces* **2012**, *4*, 296−305.
(20) (a) Bühler, G.; Feldmann, C. *Angew. Chem., Int. Ed.* **2006**, *45*, 4864−4867. (b) Hui, J.; Yu, Q.; Long, Y.; Zhang, Z.; Yang, Y.; Wang, P.; Xu, B.; Wang, X. *Chem.—Eur. J.* **2012**, *18*, 13702−13711.
(21) (a) Méndez-Vivar, J.; Mendoza-Bandala, A. *J. Non-Cryst. Solids* **2000**, *261*, 127−136. (b) Yu, M.; Lin, J.; Fang, J. *Chem. Mater.* **2005**, *17*, 1783−1791. (c) Xiao, Y.; Wu, D.; Jiang, Y.; Liu, N.; Liu, J.; Jiang, K. *J. Alloys Compd.* **2011**, *509*, 5755−5760.
(22) Yu, M.; Lin, J.; Wang, Z.; Fu, J.; Wang, S.; Zhang, H. J.; Han, Y. C. *Chem. Mater.* **2002**, *14*, 2224−2231.
(23) (a) Duan, C.; Zhang, Z.; Rösler, S.; Rösler, S.; Delsing, A.; Zhao, J.; Hintzen, H. T. *Chem. Mater.* **2011**, *23*, 1851−1861. (b) Geng, D.; Li, G.; Shang, M.; Yang, D.; Zhang, Y.; Cheng, Z.; Lin, J. *J. Mater. Chem.* **2012**, *22*, 14262−14271.
(24) (a) Li, Y.-C.; Chang, Y.-H.; Lin, Y.-F.; Lin, Y.-J.; Chang, Y.-S. *Appl. Phys. Lett.* **2006**, *89*, 081110. (b) Grzyb, T.; Lis, S. *Inorg. Chem.* **2011**, *50*, 8112−8120. (c) Inaguma, Y.; Muronoi, T.; Sano, K.; Tsuchiya, T.; Mori, Y.; Katsumata, T.; Mori, D. *Inorg. Chem.* **2011**, *50*, 5389−5395.
(25) Blasse, G.; Grabmarier, B. C. *Luminescent Materials*; Springer-Verlag: Berlin, Germany, 1994; p 96.
(26) (a) Uheda, K.; Maruyama, T.; Takizawa, H.; Endo, T. *J. Alloys Compd.* **1997**, *262*−*263*, 60−64. (b) Morell, A.; El Khiati, N. *J. Electrochem. Soc.* **1993**, *140*, 2019−2022.
(27) (a) Ding, W.; Wang, J.; Liu, Z.; Zhang, M.; Su, Q.; Tang, J. *J. Electrochem. Soc.* **2008**, *155*, J122−J127. (b) Costa, G. K. B.; Pedro, S. S.; Carvalho, I. C. S.; Sosman, L. P. *Opt. Mater.* **2009**, *31*, 1620−1627.
(28) (a) Ghosh, P.; Kar, A.; Patra, A. *Nanoscale* **2010**, *2*, 1196−1202. (b) Liu, W.-R.; Chiu, Y.-C.; Yeh, Y.-T.; Jang, S.-M.; Chen, T.-M. *J. Electrochem. Soc.* **2009**, *156*, J165−J169. (c) Tang, W.; Fu, T.; Deng, K.; Wu, M. *Ceram. Int.* **2013**, *39*, 6363−6367.
(29) (a) Geng, D.; Shang, M.; Zhang, Y.; Lian, H.; Lin, J. *Dalton Trans.* **2013**, *42*, 15372−15380. (b) Liu, Y.; Hao, J.; Zhuang, W.; Hu, Y. *J. Phys. D: Appl. Phys.* **2009**, *42*, 245102.
(30) (a) Kwon, K. H.; Im, W. B.; Jang, H. S.; Yoo, H. S.; Jeon, D. Y. *Inorg. Chem.* **2009**, *48*, 11525−11532. (b) Sinha, G.; Patra, A. *Chem. Phys. Lett.* **2009**, *473*, 151−154. (c) Mandal, S.; Bhattacharyya, S.; Borovkov, V.; Patra, A. *J. Phys. Chem. C* **2012**, *116*, 11401−11407. (d) Ruan, Y.; Xiao, Q.; Luo, W.; Li, R.; Chen, X. *Nanotechnology* **2011**, *22*, 275701.
(31) (a) Dexter, D. L. *J. Chem. Phys.* **1953**, *21*, 836−850. (b) Blasse, G. *Philips Res. Rep.* **1969**, *24*, 131−144.
(32) (a) Xie, R.-J.; Hirosaki, N.; Suehiro, T.; Xu, F.-F.; Mitomo, M. *Chem. Mater.* **2006**, *18*, 5578−5583. (b) Yeh, C.-W.; Chen, W.-T.; Liu, R.-S.; Hu, S.-F.; Sheu, H.-S.; Chen, J.-M.; Hintzen, H. T. *J. Am. Chem. Soc.* **2012**, *134*, 14108−14117. (c) Krings, M.; Montana, G.; Dronskowski, R.; Wickleder, C. *Chem. Mater.* **2011**, *23*, 1694−1699.
(33) (a) Zhang, X.; Gong, M. *Mater. Lett.* **2011**, *65*, 1756−1758. (b) Liu, W.-R.; Huang, C.-H.; Yeh, C.-W.; Tsai, J.-C.; Chiu, Y.-C.; Yeh, Y.-T.; Liu, R.-S. *Inorg. Chem.* **2012**, *51*, 9636−9641.
(34) (a) Huang, Y.; Nakai, Y.; Tsuboi, T.; Seo, H. J. *Opt. Express* **2011**, *19*, 6303−6311. (b) Orive, J.; Balda, R.; Fernández, J.; Lezama, L.; Arriortua, M. *Dalton Trans.* **2013**, *42*, 12481−12494.
(35) Zhu, G.; Ci, Z.; Wang, Q.; Wen, Y.; Han, S.; Shi, Y.; Xin, S.; Wang, Y. *J. Mater. Chem. C* **2013**, *1*, 4490−4496.
(36) (a) Choe, J. Y.; Ravichandran, D.; Blomquist, S. M.; Morton, D. C.; Kirchner, K. W.; Ervin, M. H.; Lee, U. *Appl. Phys. Lett.* **2001**, *78*, 3800−3802. (b) Li, G.; Li, C.; Zhang, C.; Cheng, Z.; Quan, Z.; Peng, C.; Lin, J. *J. Mater. Chem.* **2009**, *19*, 8936−8943.
(37) (a) Duan, C. Y.; Chen, J.; Deng, S. Z.; Xu, N. S.; Zhang, J. H.; Liang, H. B.; Su, Q. *J. Vac. Sci. Technol., B* **2007**, *25*, 618−622. (b) Xu, X. G.; Chen, J.; Deng, S. Z.; Xu, N. S.; Lin, J. *J. Vac. Sci. Technol., B* **2010**, *28*, 490−494.